AGU PUBLICATIONS

JGR

Journal of Geophysical Research: Solid Earth

RESEARCH ARTICLE

10.1002/2014JB011333

Key Points:

- Variation in gas transport properties seen with fault angle
- Repeatable gas entry pressure observed; postentry permeability varied
- Shear not an effective self-sealing mechanism to gas flow

An experimental study of the flow of gas along synthetic faults of varying orientation to the stress field: Implications for performance assessment of radioactive waste disposal

Robert J. Cuss[1], Jon F. Harrington[1], David J. Noy[1], Shanvas Sathar[2], and Simon Norris[3]

[1]British Geological Survey, Nottingham, UK, [2]Now at Department of Earth Sciences, Durham University, Durham, UK, [3]Radioactive Waste Management Limited, Didcot, UK

Correspondence to:
R. J. Cuss,
rjcu@bgs.ac.uk

Citation:
Cuss, R. J., J. F. Harrington, D. J. Noy, S. Sathar, and S. Norris (2015), An experimental study of the flow of gas along synthetic faults of varying orientation to the stress field: Implications for performance assessment of radioactive waste disposal, *J. Geophys. Res. Solid Earth*, *120*, 3932–3945, doi:10.1002/2014JB011333.

Received 2 JUN 2014
Accepted 8 FEB 2015
Accepted article online 13 FEB 2015
Published online 4 MAY 2015

Abstract Critical stress theory states that fault transmissivity is strongly dependent upon orientation with respect to the stress tensor. This paper describes an experimental study aimed at verifying critical stress theory using a bespoke angled shear rig designed to examine the relationship between gas flows along a kaolinite-filled synthetic fault as a function of fault dip. A total of 22 gas injection experiments were conducted on faults oriented 0°, 15°, 30°, and 45° to horizontal; both with and without active shear. Gas flow was seen to be complex; repeat gas injection testing showed a consistent gas entry pressure but considerably different, nonrepeatable, gas peak or breakthrough pressure. Gas flow occurred along discrete, dilatant pathways. The physics governing the pressure at which these features formed was repeatable; however, permeability was dependent on the number, distribution, and geometry of the resultant pathways. The nonrepeatable gas response suggests that the number of pathways was dependent on very subtle variations in gouge properties. No fault orientations were seen to exhibit nonflow characteristics, although critical stress theory predicted that two of the investigated fault angles should be effective seals. However, a small variation in gas entry pressure was seen with fault angle as a result of varying normal and shear stress acting on the gouge material. Shear was seen to enhance gas movement by reducing gas entry pressure and increased permeability once gas became mobile. Therefore, in kaolinite gouge-filled faults, shear is not an effective self-sealing mechanism to gas flow.

1. Introduction

Discontinuities (fractures, faults, joints, interfaces, etc.) play a pivotal role in controlling the movement of water and gas around an underground Geological Disposal Facility (GDF) for radioactive waste. High Level Waste, Intermediate Level Waste, and some long-lived low-level radioactive waste and spent fuel are planned to be disposed of in a GDF within stable geological formations at depth (~50–800 m) by a number of countries. The radioactive waste is securely isolated and contained by the engineered and geological barriers at such a facility. At depth the rock mass may be a naturally fractured environment, as in the case for crystalline rocks, and the excavation of the GDF is recognized to induce additional fractures in both crystalline and clay-rich host rocks [*Bossart et al.,* 2002; *Rutqvist et al.,* 2009]. Therefore, most current disposal concepts will result in the formation of a multitude of discontinuities as part of the natural and engineered environment. Depending on the in situ stress conditions, preferential pathways may form along any, or all, of these discontinuities.

Gas and water are expected to play a significant role in the transport of radionuclides away from the GDF. The conductivity of fluids through discontinuities is understood to be controlled by the interplay of their orientation and stress tensor direction [*Barton et al.,* 1995; *Finkbeiner et al.,* 1997]. Around the GDF there are two distinct zones with differing discontinuity orientation, discontinuity densities, and fluid flow properties: (a) the Engineered Disturbed Zone (EDZ) where an intricate range of discontinuity orientations is present in a complex localized stress field and (b) the far-field zone where discontinuous (prefractured/faulted) host rock may be present.

It has been proposed that discontinuities that are oriented parallel to the maximum horizontal stress orientation (σ_H) experience the lowest normal stresses acting across them and therefore will undergo the least amount of closure and will thus be the most permeable [*Heffer and Lean,* 1993]. This is based on

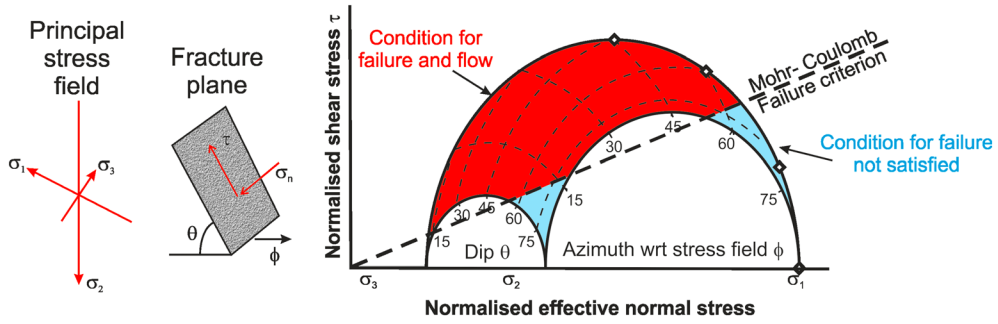

Figure 1. The three-dimensional Mohr diagram displaying the horizontal stress and normal stress on faults with respect to the in situ stress field. The points lying above the Mohr-Coulomb failure criterion are critically stressed and are likely to be conductive. Conversely, the points lying below the Mohr-Coulomb failure criterion have not reached the condition for failure and hence will be impermeable to fluid flow. Data points are shown for the four fault orientations investigated in the current study.

the assumption that discontinuities experiencing the least amount of stress will offer minimal resistance to flow. However, observations by *Laubach et al.* [2004] on a number of sedimentary basins in the western United States showed that at a depth of >3 km, the open discontinuities were not aligned parallel to σ_H. *Barton et al.* [1995] proposed that discontinuities whose state of stress was close to the failure criterion were more likely to be conductive because of localized shear failure. Such features were termed "critically stressed" and were oriented approximately 30° to σ_H. In order to apply the critical stress theory to the study of flow, the in situ stress field acting along all discontinuities in a volume of rock can be resolved into shear and normal stress components [*Rogers*, 2003; *Rogers and Evans,* 2002]. When shear and normal stresses are plotted with respect to the in situ stress field in a Mohr space, the faults and fractures that are scattered above the Mohr-Coulomb failure criterion are termed critically stressed and hence are expected to be conductive (Figure 1).

Ito and Zoback [2000] showed that the permeable faults and fractures between 3 and 7 km depth in the KTB (Kontinentales Tiefbohrprogramm der Bundesrepublik Deutschland—German Continental Deep Drilling Program) borehole were aligned close to the Mohr-Coulomb failure envelope for a coefficient of friction of 0.6. They concluded that critically stressed fractures in the crust are the most conductive to fluid flow. *Berge et al.* [1999] modeled the geomechanical behavior of the Topopah Springs tuff, Yucca Mountain, Nevada, by applying the concept of critical stress theory. Their thermohydromechanical modeling showed a factor of 2 increase in permeability for vertical fractures and up to a factor of 4 increase in permeability for fractures with slip movement. A review of the role of hydromechanical coupling in fractured rock engineering by *Rutqvist and Stephansson* [2003] concluded that stress-dependent permeability plays a major role in rocks containing flat microcracks and macrofractures. They suggested that the fracture permeability under varying stress conditions depends on hydraulic properties such as fracture permeability and connectivity of the fracture network and also on mechanical parameters such as fracture normal stiffness and fracture shear strength.

Talbot and Sirat [2001] studied the hydraulic conductivity in the highly fractured diorite at the Äspö Hard Rock Laboratory in Sweden. Out of 11,000 fractures studied, only 8% were conductive during initial excavation. The majority of the wet fractures were either subhorizontal, which were prone to thrusting, or subvertical with an underlying stress regime susceptible to wrench faulting. They concluded that faults favorably oriented for slip or dilation in the ambient stress field were most conductive to fluid flow. Similar observations were reported in the case of groundwater flow in Monterey Formation, Santa Maria Basin, California, by *Finkbeiner et al.* [1997] and in the vicinity of Yucca mountain, Nevada, by *Ferrill et al.* [1999].

Evans [2005] evaluated the fluid flow properties of critically stressed fractures in a 3.5 km deep borehole in granite at the Soultz-sous-Forets Hot Dry Rock site in the Rhinegraben area in France. All 18 naturally flowing fractures were critically stressed. However, a significant number (~500) of fractures were nonconductive irrespective of being critical stressed. Evans concluded that being critically stressed is a necessary condition for fracture flow but not a sufficient criterion for identifying flowing fractures.

Matilla and Tammisto [2012] showed that the critical stress theory could not be used to predict which of the fractures within the crystalline basement of Fennoscandian shield in the Olkiluoto Island (Finland) were conductive. A total of 38,703 fractures were examined, and between a depth range of 0 and 300 m the

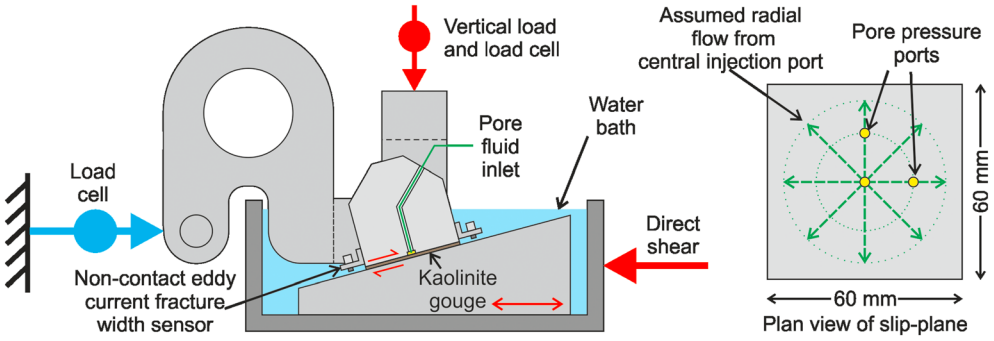

Figure 2. Schematic of the Angled Shear Rig (ASR) experimental apparatus.

majority of the conductive fractures were critically stressed. However, at depths of 300 to 800 m almost all conductive fractures lay significantly below the critical stress criterion. They concluded that the transmissivity of fluids along fractures is determined by the normal traction acting across the fractures and suggested the integrated use of contemporary stress state in addition to slip and dilation tendency analysis of the fractures to predict fluid flow.

The concept of critical stress has been widely applied to fluid flow through faults in many geological settings. The relationship between critically stressed faults and fluid flow from field studies has been inconclusive. Moreover, the occurrence of flowing fractures under noncritically stressed conditions, and conversely, the presence of nonflowing fractures in critically stressed rocks called for an experimental investigation of fluid flow along faults with different orientations with respect to σ_H and under conditions of shear movement.

The objective of this experimental program was to examine the gas flow properties of a synthetic fault at a range of fault orientations under identical boundary conditions (vertical stress). By varying fault angle with respect to a static boundary condition, this work aimed to identify fault orientations that are likely to be preferential pathways, taking into account the different resolved normal and shear stresses acting along the fault at different orientations. In addition, gas flow properties (permeability) and the pressure at which gas became mobile were investigated. Previous experimental work at the British Geological Survey (BGS) on fracture transmissivity in Opalinus clay [*Cuss et al.,* 2011] showed that hydraulic flow is a complex, focused, and transient property that is dependent upon normal stress, shear displacement, fracture topology, fluid composition, and clay swelling characteristics. The current experimental program aimed to extend this knowledge by investigating the influence of discontinuity orientation on gas flow through gouge-filled faults. Figure 1 shows the stress state of the four fault orientations investigated in the current study with the Mohr-Coulomb envelope, using a coefficient of friction of 0.37 for pure kaolinite [*Crawford et al.,* 2008]. This predicts that the synthetic faults oriented 0° and 15° to the horizontal should be effective seals, while the synthetic faults oriented 30° and 45° to the horizontal should be conduits of flow.

2. Experimental Setup

All experiments were performed using the bespoke Angled Shear Rig (ASR, Figure 2) designed and built at BGS. Previous experiments conducted on Opalinus clay [*Cuss et al.,* 2011] showed that fracture topology is a key parameter in controlling fluid flow along fractures. In order to reduce the number of variables required to fully understand flow, a "generic" synthetic fault with smooth surfaces was investigated.

The ASR (Figure 2) composed of five key components: (1) Rigid frame that had been designed to deform as little as possible during the experiment; (2) vertical load system comprising an Enerpac hydraulic ram that was controlled using a Teledyne/ISCO 260D syringe pump, a rigid loading frame, and an upper thrust block (up to 20 MPa normal stress, 72 kN force). The Enerpac ram had a stroke of 105 mm, which meant that it could easily accommodate the vertical displacement of the top block as it rode up the fault surface at constant vertical load; (3) shear force actuator composed of a modified and horizontally mounted Teledyne/ISCO 500D syringe pump designed to drive shear as slow as 14 μm a day at a constant rate (equivalent to 1 mm in 69 days) or as fast as 0.5 mm per second along a low friction bearing; (4) pore pressure system comprising a Teledyne/ISCO 500D syringe pump that could deliver either water or gas up to a pressure of 25.8 MPa.

The syringe pump delivered water into the base of a water/gas interface vessel, which injected helium gas through the center of the top block directly to the fault surface. And (5) a state-of-the-art custom designed data acquisition system using National Instruments LabVIEW™ software facilitating the remote monitoring and control of all experimental parameters.

The experimental fault assembly consisted of precision machined 316 stainless steel top and bottom blocks (thrust blocks) with dips of 0°, 15°, 30°, and 45° with respect to horizontal. This allowed the pure mechanical influence of discontinuity orientation on gas flow to be investigated in a simplified system. The thrust blocks were polished so as not to introduce preferential gas pathways for flow. The top block was connected to the vertical loading mechanism by means of a swivel mechanism which was engaged to the shoulders on either side of the top block. Two pore pressure transducers, attached to ports, which were positioned orthogonally to each other at 15 mm from the central pore fluid inlet, allowed measurement of pore pressures within the fault gouge (see Figure 2). The upper thrust blocks of the apparatus were made with a contact area of 60 mm × 60 mm. The lower thrust block was longer than the top one so that the contact area of the experimental discontinuity could be maintained constant throughout the test.

As shown in Figure 2, the shear force actuator acted upon the angled bottom block of the apparatus. The movement of the bottom block was measured using a linear variable differential transformer, which had a full range of ±25 mm and an accuracy of 0.5 μm. Vertical travel of the thrust block was measured by a high-precision noncontact capacitance displacement transducer, which had a full range of ± 0.5 mm and an accuracy of 0.06 μm. Two high-precision eddy current noncontact displacement transducers either end of the top thrust block recorded gouge thickness directly and determined nonparallel alignment of the two thrust blocks. These submersible devices had a full range of ± 1 mm and an accuracy of 0.2 μm. Horizontal load was measured using a load cell fitted laterally to the top block. This measured the force resultant from lateral movement of the bottom block transmitted through the clay gouge.

Gouge material for the experiments was prepared from powdered kaolinite (Supreme Powder); 16 ± 0.1 g of deionized water was added to 20 ± 0.1 g of kaolinite powder. The water and kaolinite were then stirred for 5 min giving a kaolinite paste with a gravimetric water content of 80 ± 1%. The paste was smeared uniformly onto the surface of the top block, which was then carefully lowered onto the bottom block thus forming a kaolinite paste gouge. The initial thickness of the gouge was measured to be ~1 mm. However, as no lateral confinement was made of the clay gouge, thickness decreased to approximately 70 ± 10 μm with loading, and clay was squeezed from between the thrust blocks. The apparatus was designed without lateral gouge confinement as this would require sealing elements that would have a high frictional component along the fault surface compared with the low frictional properties of kaolinite. Initial loading resulted in excess clay being squeezed out from the fault surface; this excess material prevented water from the shear bath entering the fault gouge or from causing sloughing.

All gas injection experiments (Table 1) were performed at a hydraulic jack pressure of 10 MPa, giving a vertical stress of 4.3 MPa (1570 kg force). The gas injection rate was controlled using a Teledyne/ISCO pump from a starting gas pressure of 4 MPa. It should be noted that the starting volume of gas within the water/gas interface vessel was 200 ± 0.2 cm^3 (at 4 MPa pressure) in all experiments. Gas injection was performed by injecting water into the gas/water interface vessel through the bottom inlet at a flow rate of 700 μL h^{-1}. This pressurized and pushed gas through the outlet at the top of the interface vessel and directly into the fault gouge once the gas entry pressure had been achieved.

2.1. Data Reduction

Gas pressure can be predicted using Boyle's law. The starting volume (V_1) and pressure (P_1) of gas can be determined through the careful setup of the pore pressure system. The syringe pump used displaces a known volume (±1 μL) of water into a water/gas interface vessel. At all times during the gas injection test the volume of the gas in the interface vessel (V_2) is thus known. Therefore, from the expression

$$P_1 V_1 = P_2 V_2 \tag{1}$$

the gas pressure is predicted as

$$P_2 = \frac{P_1 V_1}{V_2} \tag{2}$$

Table 1. List of All Experiments Undertaken as Part of the Current Study[a]

Experiment	Test Type	Slip Plane Orientation	Gas Entry Pressure (MPa)	Average Gas Entry Pressure (MPa)	Gas Peak Pressure (MPa)
ASR_Tau15_00gGI	Gas injection test	0°	*5.0*	8.4 ± 0.8	(8.05)
ASR_Tau16_00gGI	without shear		8.0		(17.7)
ASR_Tau17_00gGI			9.0		14.95
ASR_Tau21_00gGI			7.5		(13.98)
ASR_Tau22_00gGI			9.25		/
ASR_Tau18_15gGI		15°	7.5	7.6 ± 0.1	11.8
ASR_Tau19_15gGI			7.5		8.1
ASR_Tau20_15gGI			7.75		(11.7)
ASR_Tau09_30gGI		30°	*5.2*	7.7 ± 0.6	8.2
ASR_Tau11_30gGI			8.0		(15.5)
ASR_Tau12_30gGI			7.0		11.0
ASR_Tau13_30gGI			8.0		(13.55)
ASR_Tau25_45gGI		45°	8.5	8.0 ± 0.7	(14.9)
ASR_Tau26_45gGI			7.5		(9.25)
ASR_Tau27_45gGI			*5.0*		(8.2)
ASR_Tau23_00gGI	Elevated injection rate	0°	7.0	7.5 ± 0.7	(24.85)
ASR_Tau24_00gGI			8.0		(25.5)
ASR_Tau28_00gGIS	Gas injection test		5.5	5.6 ± 0.4	7.30
ASR_Tau29_00gGIS	with active shear		6.0		8.22
ASR_Tau32_15gGIS		15°	5.25	5.2	10.75
ASR_Tau30_30gGIS		30°	7.0	7.0	(13.5)
ASR_Tau31_45gGIS		45°	5.0	5.0	8.35

[a]Gas peak pressure values in brackets represent maximum gas pressure recorded in tests where peak pressure was not achieved.

The mass flux of gas per unit time into the clay gouge at any point during the gas injection history can be simply derived using a data reduction algorithm based on the ideal gas law. At any point in time, the total volume of the injection system V_s is

$$V_s = V_w + V_g \tag{3}$$

where V_w and V_g are the volume of water and gas, respectively. It should be noted that it is possible to correct for compressibility of the test apparatus and compression of the water. However, in previous laboratory tests these corrections have been extremely small, and in the absence of representative data, it was felt inappropriate to apply such a correction.

As the injection pump advances (i.e., water is injected into the interface vessel), the volume of gas reduces by an equal amount as compression of the gas occurs, i.e.,

$$V_g(t) = V_s - V_g(t) \tag{4}$$

The ideal gas law states that

$$PV_g = nRT \tag{5}$$

where P is the gas pressure (Pa), n is the number of moles of gas in the system, R is the universal gas constant (taken as 8.3 $J\,K^{-1}\,mol^{-1}$), and T is ambient temperature (K). Thus, the number of moles of gas injected into the clay can be calculated from

$$n_{t=0} - n_t = \frac{P_{t=0}V_g(t=0) - P_tV_g(t)}{RT} \tag{6}$$

By multiplying equation (5) by the molar volume of gas (taken as 0.02241 $m^3\,mol^{-1}$) defined at standard temperature and pressure (STP) conditions (defined as 273.15 K and 101.325 kPa), the equivalent volumetric flow rate of gas (at STP conditions) injected into the buffer clay can be obtained.

It should be noted that the calculation procedure outlined above is extremely sensitive to the start volume of gas. Minor errors in this parameter can have significant effects on the calculation of gas flows and the subsequent interpretation of the data; this is minimized through the careful filling of the interface vessel with a known volume of gas.

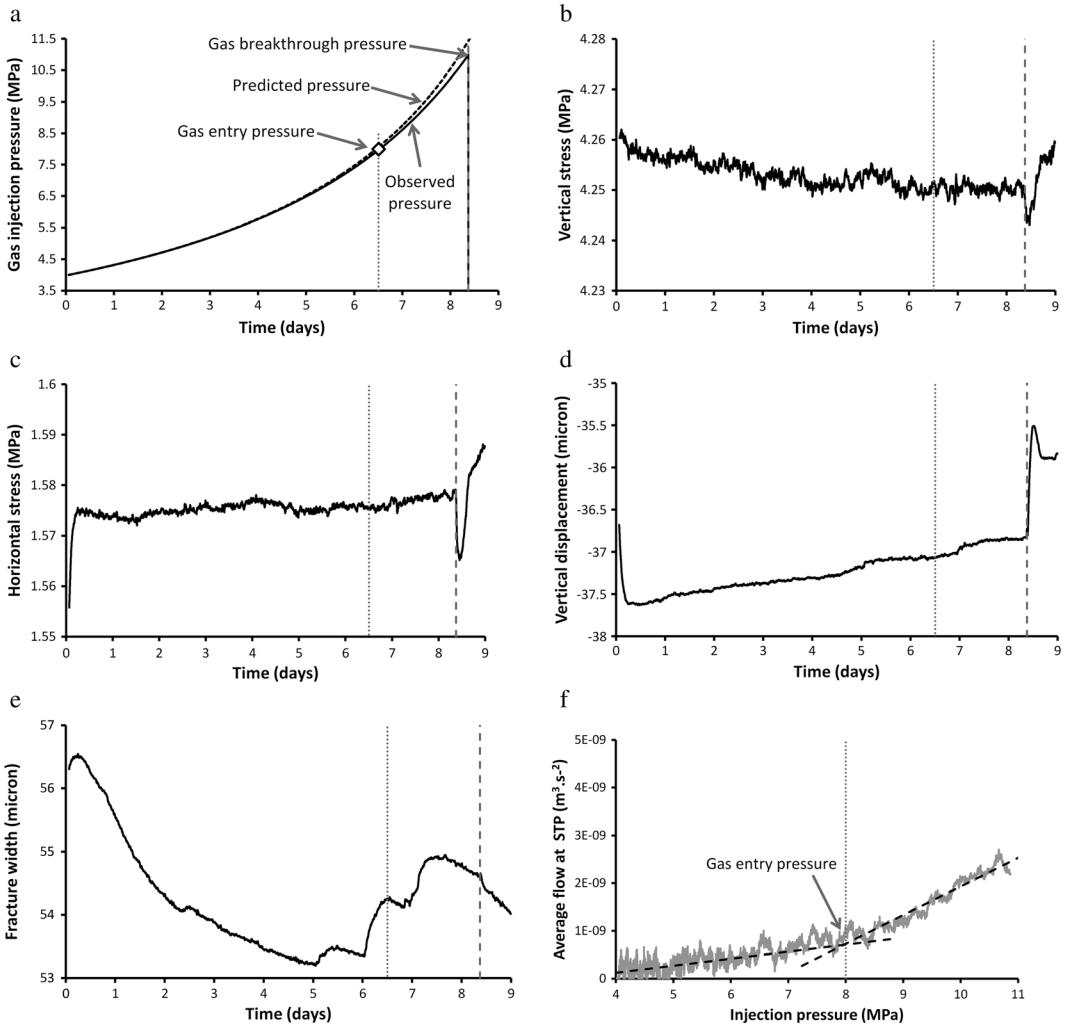

Figure 3. Example test results for test ASR_Tau12_30gGl; (a) Gas injection pressure compared with prediction from Boyle's law, (b) vertical stress, (c) horizontal stress, (d) vertical displacement, (e) fracture width, and (f) flow into the fault gouge as a way of predicting gas entry pressure.

The average flow at STP into the fracture was calculated using equation (6). As shown in Figure 3f, the flow rate is initially very small and rising gradually, but then the rate of increase of the flow rate abruptly increases. The pressure at which this occurs is identified as the gas entry pressure. Gas peak pressure is simply the maximum gas pressure experienced. Gas breakthrough is the pressure when gas was able to reach the outside of the top block, resulting in a reduction in gas pressure.

3. Experimental Results

A total of 22 near-identical gas breakthrough experiments were conducted on discontinuities oriented 0°, 15°, 30°, and 45° to the horizontal; both with (five tests) and without (17 tests) active shear (see Table 1). Two tests were conducted with an increased gas pressurization rate in order to investigate the rate-dependent effects; these were performed with a flow rate of 1400 $\mu L\,h^{-1}$. All tests are described in detail in *Cuss et al.* [2013].

3.1. Gas Injection Experiments Without Shear

A total of 15 gas injection experiments were conducted without active shear. Figure 3 shows typical data from test ASR_Tau12_30gGl conducted on a fault oriented 30° to the horizontal. As can be seen in Figure 3a, the gas injection experiment resulted in a maximum gas pressure, equivalent to the breakthrough pressure,

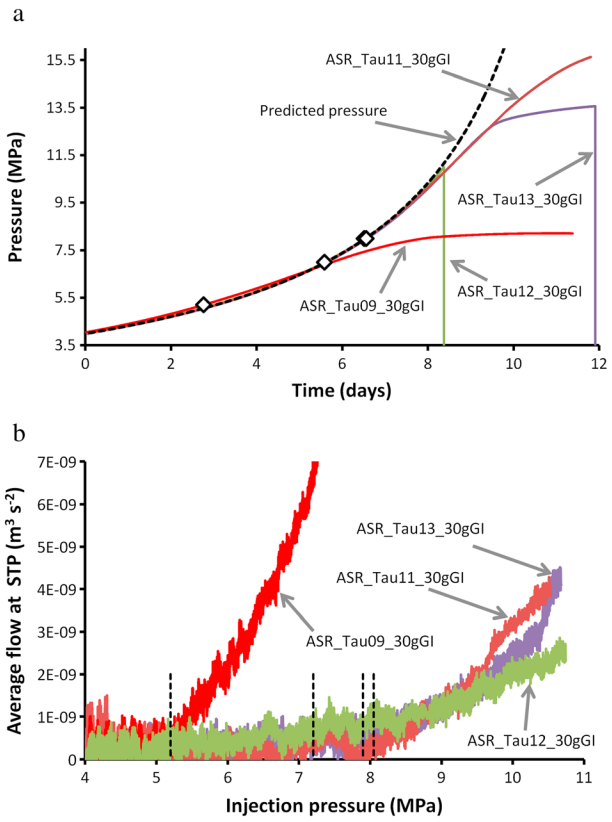

Figure 4. Repeatability example of gas injection test results for four gas injection tests conducted on a fracture oriented at 30° to horizontal; (a) gas pressure response. As can be seen, considerable differences are seen in peak pressure and form of the curve indicating that fault gouge transmissivity is not repeatable; (b) gas entry pressure predicted from the average flow at STP. As can be seen, repeatable gas entry pressure is seen for three of the four tests, with one test showing a considerably lower gas entry pressure.

of approximately 11 MPa, followed by a total loss of gas pressure as the fault gouge became highly conductive. Throughout the test vertical stress (Figure 3b) was maintained at approximately 4.3 MPa, with a resultant measured horizontal stress of 1.57 MPa (Figure 3c). The normal displacement data (Figure 3d) showed that the fracture dilated initially and following this compressed throughout the rest of the test. As can be seen, a significant contraction event was seen at the time of the gas breakthrough. The eddy current sensor measuring fracture thickness showed a complex history (Figure 3e). As seen in the normal displacement sensor, dilation was initially observed, followed by compression, with dilatant episodes beginning around Day 5. These observations do not appear to correlate with any features seen in stress, vertical displacement, or flow. However, one of the dilatant features does correspond approximately with the identified gas entry. Figure 3f shows the average flow at standard temperature and pressure (STP) into the fracture, with gas entry inferred to be approximately 8.0 MPa.

Nonrepeatability is problematic during any experimentation. Figure 4 shows an example of the repeatability of experimental results for four tests conducted on a fault oriented at 30° to the horizontal. The gas flow/breakthrough results achieved at this orientation are typical of the variability observed for all orientations investigated (see Figure 5) in the present study. A defined peak pressure of approximately 8 MPa was achieved in test ASR_Tau09_30gGI (Figure 4a). Similarly, experiment ASR_Tau13_30gGI showed a peak pressure of 13.6 MPa, followed by gas flow and a loss of pressure as the gouge layer became conductive (gas breakthrough). During test ASR_Tau11_30gGI a peak pressure was not achieved, with a resultant gas pressure of approximately 15.5 MPa. The form of the pressure response suggests a peak pressure of 18 MPa may have been achieved had it been possible to run the experiment to higher pore fluid pressures. Test ASR_Tau12_30gGI showed a distinct dilation event at gas breakthrough; in contrast, no dilation was seen at the time of gas breakthrough in test ASR_Tau13_30gGI. It can be seen that the pressure response for three of the tests (ASR_Tau11_30gGI, ASR_Tau12_30gGI, and ASR_Tau13_30gGI) show similar behavior until the gas entry pressure, following which two tests achieved gas breakthrough. As shown in Figure 4a there is little repeatability in the gas pressures achieved with maximum pressures of between 8 and 16 MPa in tests that were conducted under identical boundary conditions.

Nonrepeatable gas pressure response described for a discontinuity oriented at 30° was not unique to this set of tests, as shown in Figure 5. All discontinuity orientations show considerable spreads in gas pressures; at 0°, 15°, 30°, and 45° orientations, the variations in gas entry pressures were 9.7 MPa (8–17.7 MPa), 3.6 MPa (8.2–11.8 MPa), 7.4 MPa (8.2–15.6 MPa), and 6.8 MPa (8.2–15 MPa), respectively. This shows a total spread of gas peak pressures between 8 and 17.7 MPa. As can be seen in Figure 5, there is no systematic relationship between achieved gas pressure and fault orientation.

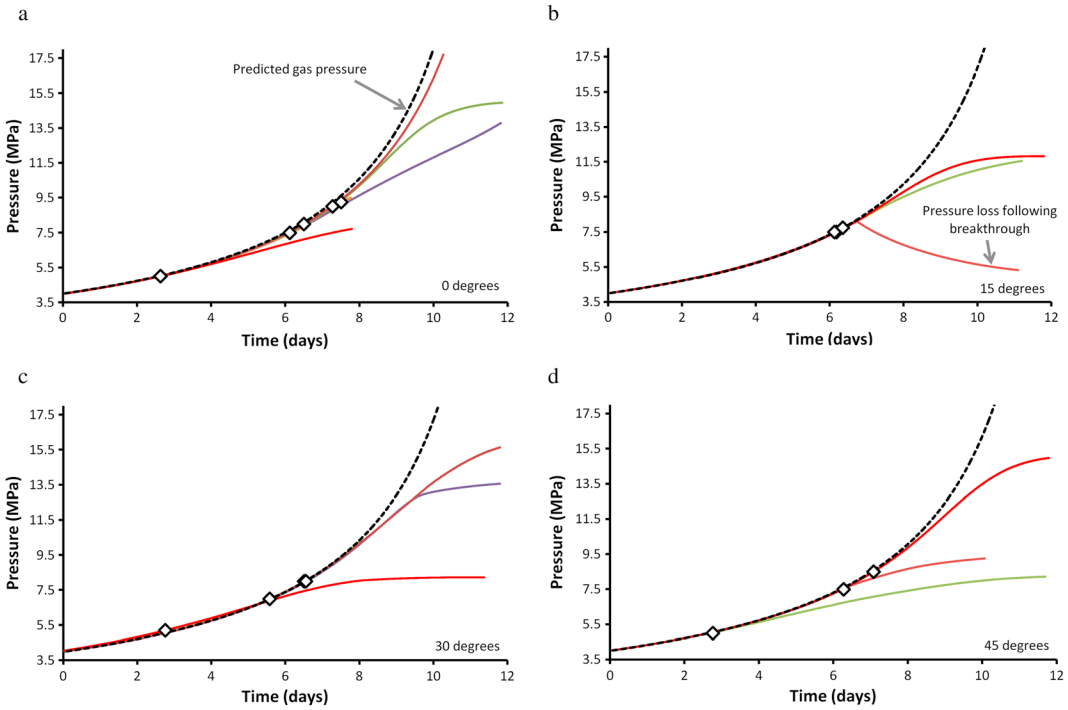

Figure 5. Repeatability of gas pressure response for all test; tests conducted at (a) 0° to the horizontal, (b) 15°, (c) 30°, and (d) 45°.

While there appears to be little repeatability in gas peak pressure, there is some correspondence in gas entry pressure. Figure 4b shows the result of average flow at STP for the four tests conducted on a discontinuity oriented 30° to the slip plane. As seen in Figure 4b three tests showed similar gas entry of approximately 8 MPa, with test ASR_Tau09_30gGI showing an anomalously low, but distinct, entry pressure of 5.5 MPa. Similar anomalously low gas entry pressures were seen for other orientations, suggesting that gas was able to exploit a "defect" of some form at a low pressure, and hence, the experiment was unable to be perfectly reproducible.

Although some tests have shown anomalously low gas entry pressures, Figure 6 shows a general variation of gas entry pressure with discontinuity orientation. All investigated orientations show considerable variation with the extreme being a discontinuity with an orientation of 0°, with an average of 8.4 ± 0.8 MPa. The other extreme was a discontinuity oriented at 15° to the slip plane, with an average of 7.6 ± 0.1 MPa. The variation in spread in results is because of a limited number of tests that showed entry at lower pressures. The highest average gas entry pressure, as expected, was seen on a horizontal slip plane with an entry pressure of almost 8.5 MPa. The lowest gas entry pressure was recorded at a slip plane orientation of 15° of 7.6 ± 0.1 MPa. Figure 6a shows two possible relationships describing the variation of flow with fault dip. A linear relationship is observed when fit to the complete data. This predicts a modest reduction in gas entry pressure with increasing dip. A parabolic relationship is also shown fit to the average gas entry pressures. This predicts that a minimum gas entry pressure occurs at 25 ± 5° to the horizontal. However, this relationship is statistically questionable given the considerable spread in the data, with the linear trend plotted in Figure 6a giving a good fit to the data.

3.2. Gas Injection Experiments With Active Shear

A further study was made of the influence of active shear on the gas transport properties of the kaolinite gouge. A total of five gas injection experiments were conducted with active shear. Two tests were conducted on a flat slip plane, i.e., at an orientation of 0° with respect to horizontal in order to assess repeatability. Further three tests were conducted at orientations of 15°, 30°, and 45° in order to investigate the relationship between active shear and gas entry pressure at different angles. As stated previously, each test was performed as near as possible identical, i.e., the same water content within the gouge, vertical stress, volumes of gas, and gas injection rates. The only parameter that is likely to have varied between tests was the thickness of the gouge

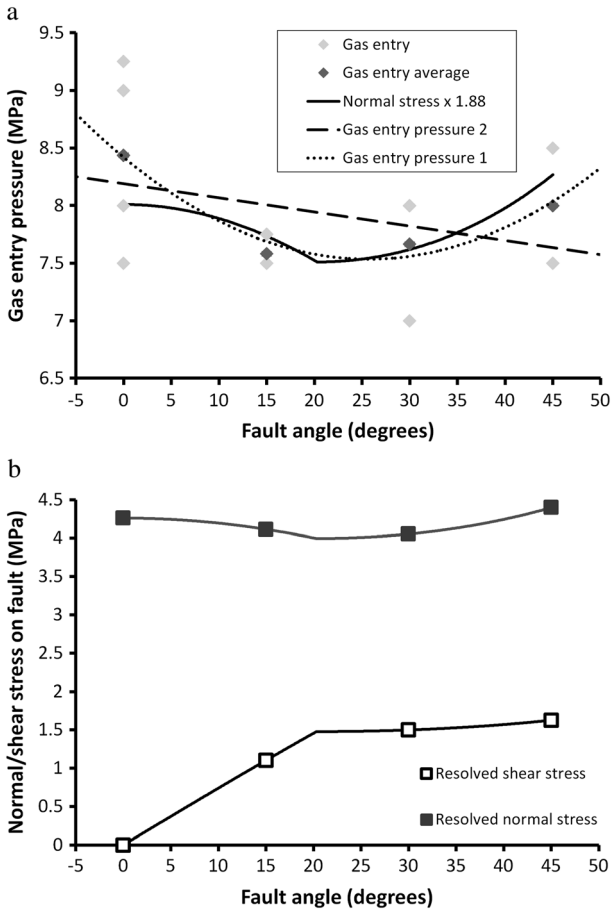

Figure 6. Relationship of gas entry pressure with fault angle: (a) gas entry pressure variation with fault angle and (b) resolved normal and shear stress acting on the fault gouge.

at the start of the experiment. However, as best as could be established, this did not vary significantly between tests as the gouge became thin in all tests as the initial load was applied.

In all tests the shearing began at the same time as the constant flow pressure ramp was started. During the active shear, the faults underwent approximately 4% strain, during which time horizontal stress in the kaolinite gouge generally doubled (Figure 7c). As can be seen in Figures 7b and 7c, shear stress reached a maximum threshold before gas entry began. Therefore, the action of active shear altered the stress state of the gouge sufficiently prior to gas entry, even though shearing and gas injection were initiated simultaneously. As with the test results presented above, active shear did not result in repeatable peak pressure or a systematic alignment of peak pressure with fault orientation. However, both tests conducted on a fault oriented 0° to the horizontal reach peak pressure conditions at relatively low pressures compared with nonsheared tests. This suggests that the process of shear-enhanced fault transmissivity as the gouge dilated during shearing, as observed in Figure 7d. Both tests reached peak pressure and decayed, whereas without shear no pressure decay was observed. As shown in Figure 7a, shear resulted in a reduction of approximately 2.5 MPa of gas entry pressure determined from average STP flow.

3.3. Gas Injection Experiments at Elevated Injection Rate

Two gas injection experiments were conducted with an increased rate of pressurization in order to investigate whether gas entry pressure and gas peak pressure are rate dependent. As stated previously, each test was performed as identically as possible and only varied by their pressurization rate. The results conducted on a fault oriented at 0° with an increased gas injection rate are shown in Figure 8a. An increased gas injection rate significantly altered the gas response of the gouge with significantly higher gas pressure achieved in excess of 24 MPa. Neither test showed signs of reaching peak pressure behavior. Given the significant change in peak pressure achieved, only a marginal change in gas entry pressure was observed; reducing from an average of 8.4 ± 0.8 to 7.5 ± 0.7 MPa when estimated from STP gas flow into the fracture. This suggested that the rate of pressurization had only a small effect on the gas entry pressure, but once gas was mobile within the kaolinite gouge, it had a considerable influence.

3.4. Observations of Gas Breakthrough in Kaolinite Gouge

Five gas injection tests were conducted with the addition of time-lapse photography in order to identify the time of gas escaping the kaolinite gouge (gas breakthrough). Gas bubbles were observed in only three of these tests. For two of the time-lapse experiments the pressure at which the first bubble was identified corresponded closely with the gas entry pressure predicted from average flow at STP into the fracture. Therefore, it is possible that this technique identifies the gas breakthrough pressure (when the gas pressure is sufficient to allow escape from the sample). However, one test showed gas bubbles did not appear until a

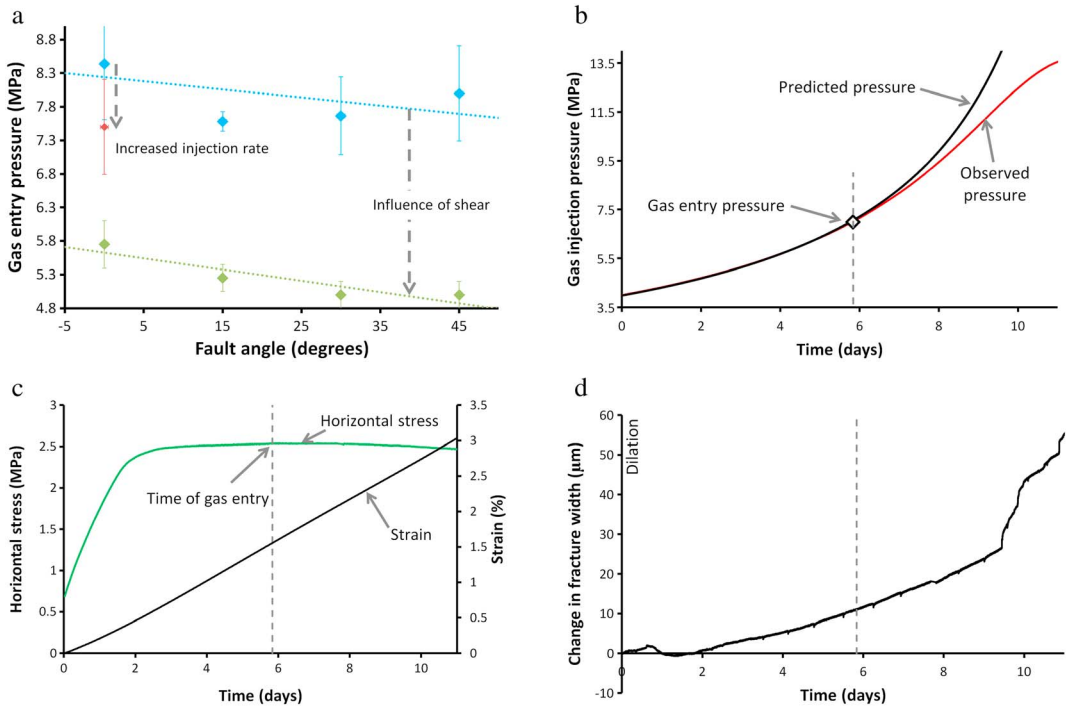

Figure 7. The influence of shear and increased injection rate on gas entry pressure; (a) variation of gas entry pressure with fault angle, (b) gas injection pressure compared with prediction from Boyle's law, (c) shear stress and strain, and (d) change in fracture width. Data for Figures 7b to 7d from test ASR_Tau30_30gGIS.

pressure greatly in excess of the gas entry pressure. This test showed that observed gas pressure was close to predicted gas pressure, suggesting that little gas had entered the gouge. Two tests did not observe gas bubbles (tests ASR_Tau20_15gGI and ASR_Tau23_00gGI), although this may be due to the limited view of the apparatus recorded by the time-lapse camera. However, test ASR_Tau23_00gGI displayed a gas pressure close to the predicted pressure, indicating that little gas had entered the gouge, and by the end of the test, this gas may not have migrated as far as the outside of the kaolinite gouge. Two tests showed that gas migrated and exited the gouge at a single point; suggesting only one pathway had facilitated gas breakthrough. However, one test showed that gas initially escaped from a single location, which soon sealed and gas then escaped from two other locations diametrically opposed on the thrust block. This suggests that multiple pathways formed and continued to evolve even following gas breakthrough.

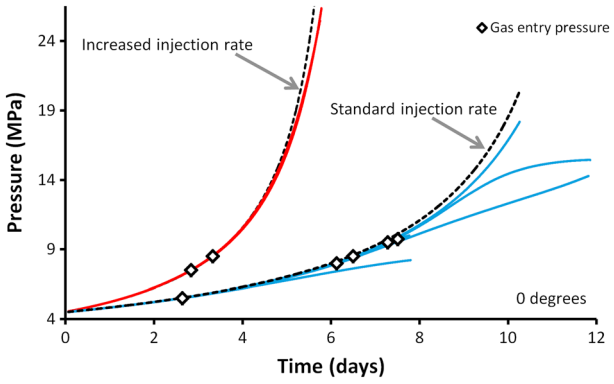

Figure 8. Pressure response from two tests conducted at a higher gas injection rate compared with five tests conducted at the standard injection rate.

In order to understand the propagation of gas through kaolinite gouge, a second apparatus was constructed (Fracture Visualization Rig [*Wiseall et al.,* 2014]). This setup employed a similar experimental geometry with a glass top block allowing gas movement to be observed within the clay gouge up to a maximum normal stress of 3 MPa. As shown in Figure 9, dilatant pathways similar to fractures were formed. *Wiseall et al.* [2014] reported the contraction of the clay around the dilating gas pathways, and when breakthrough occurred, these pathways closed as the kaolinite elastically

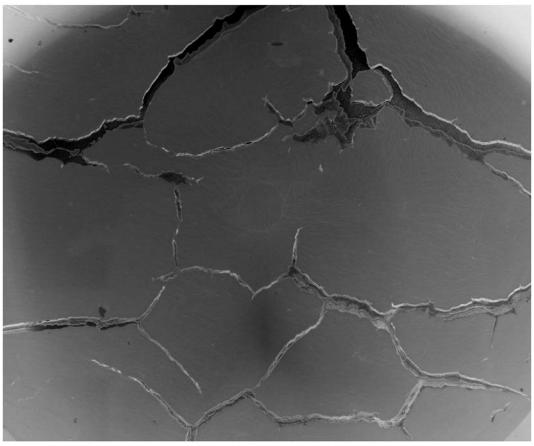

Figure 9. Time-lapse photograph showing the formation of localized dilatant gas pathways in kaolinite gouge using the Fracture Visualization Rig [from *Wiseall et al.,* 2014].

recovered in response to a reduced gas pressure within these features. The pattern of formed pathways was generally random and was not seen to be repeatable. Some tests form few pathways, while others (e.g., Figure 9) formed many features.

4. Discussion

Considerable variation was observed in achieved gas peak pressures in different experiments that were repeated as identical as possible. No systematic relationship was noted between peak pressure and fault angle. However, repeatable gas entry pressures were observed, although these did display considerable spread. These observations demonstrate that the physical control on gas entry was repeatable, although in the presence of any form of imperfection, gas was able to enter at lower pressures. Once gas started to move within the fault gouge, the progression of pressure was less predictable and depended on whether the evolving gas pathway network located an exit from the system. Similar results were seen for all fault angles investigated. The observed escape of gas through bubble streams shows that gas propagated along isolated, localized pathways. This hypothesis was further strengthened by direct visual observations of gas flow in kaolinite gouge material. A number of dilatant gas pathways were seen to form in a nonrepeatable manner. The number, distribution, and therefore volume of the features were not consistent between tests. Gas can therefore be idealized as moving along discrete "fractures" or "ruptures" in the clay matrix and is not moving through the interconnected clay porosity, as would be expected for viscocapilliary or two-phase flow; where gas movement is coupled with the displacement of water from the porous network. The observed dilatancy seen during some experiments where gas breakthrough occurred strengthens this hypothesis. With such a gas transport mechanism the pressure at which gas becomes mobile would be controlled by the physics of the clay gouge and is related to the pore throat aperture of the clay. Once gas becomes mobile, the transmissivity of the gouge is then dependent on the number, aperture, and length of the pathways formed. A gouge with a greater number of pathways will appear to have a higher transmissivity, whereas a gouge with limited pathway formation will have relatively limited transmissivity. The observed modification of gas escape from the gouge, switching from a single exit point to a dual exit system for one test, demonstrates that the pathway geometry continues to evolve, even when the gas has achieved breakthrough; this was also observed in the Fracture Visualization Rig. Elevated gas pressurization rate did not alter the gas entry pressure as the increased rate of gas pressurization would not alter the pore throat control on gas entry.

Despite the nonrepeatable flow characteristics of the gouge material tested, the experimental study has demonstrated a variation in gas entry pressure in faults with fault angle. However, the variation in gas entry pressure is only of the order of 1 MPa for a parabolic fit to the data, or 0.5 MPa for a linear fit, and was not as pronounced as anticipated given field observations [e.g., *Sathar et al.,* 2012]. Under natural field conditions the thickness and roughness of the fault surface is likely to be more than that of the idealized kaolinite gouge-filled fault used in the experiments. No fault angle tested could be described as nonflowing; however, certain orientations had greater conductivity than others. The critical stress criterion shown in Figure 1 predicted two of the tested fault angles would be sealed, while two would flow. There was no discernable variation in gas flow, other than a small reduction in gas entry pressure. Unsurprisingly the horizontal fault (0° to horizontal) showed the highest gas entry pressure. This implies that faults that are oriented at right angles to the normal stress direction will experience maximum compressive stresses and as a result have the lowest gas conductivity. Moreover, the lack of shear stress under this condition negates any opening/rotation of the clay minerals as a result of deviatoric stresses hence maintaining the sealing properties of the fault gouge.

All tests were conducted at identical vertical loads. As fault angle varies, the load acting normal and parallel to the fault will vary; this can be determined translating recorded vertical (σ_V) and horizontal (σ_H) stresses to

Table 2. Resolved Normal and Shear Stress Acting on the Fault Plane at the Test Orientations

Fault Angle (deg)	Vertical Stress (MPa)	Resolved Normal Stress on the Fault (MPa)	Resolved Shear Stress on the Fault (MPa)
0	4.26	4.26	0
15	4.26	4.11	1.1
30	4.26	4.05	1.5
45	4.26	4.4	1.63

normal (σ_n) and shear (τ) components, as shown in Figure 6 and Table 2. During the loading stage of the experiment, no acceleration is observed; there must therefore be a force balance in each direction

$$\sigma_V = \sigma_n \cos\theta + \tau \sin\theta \quad \text{and} \quad \sigma_H = \sigma_n \sin\theta + \tau \cos\theta \tag{7}$$

where Θ is the inclination of the fault with respect to the horizontal. When the gouge has not undergone yield, σ_H will equal to zero as the friction of the fault surface will be sufficient resistance to oppose sliding. Therefore,

$$\sigma_n = \sigma_V \cos\theta \quad \text{and} \quad \tau = \sigma_V \sin\theta \tag{8}$$

However, if the gouge has undergone yield, then

$$\sigma_n = \frac{\sigma_V}{\cos\theta + \mu \sin\theta} \quad \text{and} \quad \sigma_n = \frac{\sigma_H}{\sin\theta - \mu \cos\theta} \tag{9}$$

assuming Coulomb's law ($\tau = \mu \sigma_n$), where μ is the coefficient of friction, the yielding condition is $\mu < \tan\Theta$. Therefore, at angles greater than 20.3° yield will occur and stresses can be determined from (9), whereas at angles less than 20.3° yield will not occur and (8) should be used. Normal and shear stresses acting on the fault are plotted in Figure 6b.

For a flat fault the normal stress is 4.3 MPa, reducing to a low of about 4.0 MPa when the fault is 20°. The shear stress is zero for a flat fault, increasing to 4.3 MPa when the fault is 45°. If the change in gas entry pressure seen was simply due to changes in normal stress on the fault gouge as a result of fault angle, it would be expected that a similar form would be seen in the relationship of both normal stress and gas entry pressure. As shown in Figure 6a a prediction for the gas entry pressure (P_{ge}) has been achieved for the following relationship:

$$P_{ge} = 1.88\, \sigma_n \tag{10}$$

While this relationship achieves a fit to the data, it underestimates the gas entry pressure on a horizontal fault and is a simple empirical relationship. More data are required at intermediate angles in order to fully explore the relationship between normal stress and gas entry pressure. The form of shear stress with fault angle does not suggest a direct correlation between shear stress and gas entry pressure. It is probable that the gas entry pressure is dependent upon a combination of normal stress and shear stress.

Shear was seen to have a pronounced influence on the gas entry pressure, but little influence on the flow properties of the kaolinite gouge. Unexpectedly, gas entry pressure was seen to reduce by approximately 2.5 MPa following shear. In tests on Opalinus clay [*Cuss et al.,* 2011, 2012] active shear markedly reduced hydraulic fracture transmissivity by up to an order of magnitude. Therefore, it was expected that the mobility of gas in kaolinite would be impeded by shear and that gas entry pressure would increase. However, shear significantly reduced gas entry pressure and resulted in a relatively low gas peak pressure, suggesting that the mobility of gas was increased by shear. This can be explained by the observed dilation of the gouge material. This would modify pore throat size, which in turn would make gas entry easier. During shearing of Opalinus clay, the clay mineral assemblage will be smeared along the fracture surface, resulting in a more efficient hydraulic barrier. Therefore, it can be concluded that shear is not an effective self-sealing mechanism to gas in kaolinite fault gouges.

The observations from the current study have implications for the treatment of faults and fractures in the performance assessment of a GDF, especially in the EDZ and in naturally fractured host rocks where faults and fractures of diverse orientations are present. Assuming that fault gouges composed of other clay minerals behave similarly to kaolinite, shear movement along faults will result in enhanced gas flow and in the absence of free-water shearing is not an effective self-sealing mechanism. Little variation in gas entry pressure was seen at different fault angles. This shows that the prediction of conductive and nonconductive fault orientations from critical stress theory is not applicable for gas flow. Corrosion of ferrous materials under anoxic conditions,

combined with the radioactive decay of the waste and the radiolysis of water, will lead to the formation of hydrogen. If the rate of gas production exceeds the rate of gas diffusion within the pores of the barrier or host rock, a discrete gas phase will form and accumulate in the void space of the canister [*Horseman et al.,* 1999; *Ortiz et al.,* 1997; *Wikramaratna et al.,* 1993]. Gas will then enter the fault gouge when the gas pressure exceeds gas entry pressure. This study has shown that shearing along faults will aid the dissipation of this excess gas pressure, while the observed reduction in hydraulic transmissivity reported by *Cuss et al.* [2011, 2012] will act as a barrier for water to reach waste canisters, reducing the production of hydrogen. Therefore, fault shearing has a dual role in performance assessment of the long-term disposal of radioactive waste forms.

However, this study has highlighted difficulties in dealing with gas in performance assessment. The nonrepeatability of gas pressure response following gas entry as a result of differences in the number, aperture, and distribution of flow pathways makes mathematical modeling of gas flow along faults challenging. While every care was taken to create near-identical test conditions, it is unlikely that such large differences in flow properties were the result of very subtle changes in gouge properties resulting from clay gouge manufacture. A greater understanding of the formation of these pathways and the controls on their properties is required in order to mathematically predict the gas flow properties of fault gouges. This study has clearly shown that once gas is mobile, the permeability of the gouge material is not consistent between tests.

5. Conclusions

This paper describes an experimental study of 22 separate experiments with the primary aim to verify critical stress theory. Experiments were conducted on fault angles of 0°, 15°, 30°, and 45° to the horizontal; both with and without active shear. All tests were conducted in an identical manner. Critical stress theory predicted that the faults oriented 0° and 15° were noncritical and should therefore be barriers to flow, while the faults oriented 30° and 45° should be conductive. Gas injection experiments were conducted, where gas pressure was increased in a pressure ramp at constant vertical load. Repeat gas injection testing showed a consistent gas entry pressure but considerably different, nonrepeatable, and gas peak pressures. Observations suggest that gas flow was along discrete, dilatant pathways. The physics governing gas entry, the point at which gas is able to move through the kaolinite gouge, was seen to be repeatable and was related to pore throat size in the clay gouge. However, once gas pathways were forming and pathway networks were evolving the gas transport properties were dependent on the number, aperture, and length of these features. The nonrepeatable gas response suggests that the number of formed pathways was dependent on very subtle variations in gouge properties.

Our observations suggest that the critical stress theory is valid in terms of suggesting that the gas transport properties (gas entry pressure) of faults at different orientations do vary. However, the variation was limited, and the condition of nonflowing faults was not observed. Only a small change in gas entry pressure was seen, and this was due to variations in normal and shear stress in the fault gouge, resulting in changes in the pore geometry of the clay. A relationship between normal stress and gas entry pressure ($P_{ge} = 1.88\ \sigma_n$) has been hypothesized. Shear was seen to enhance gas movement by reducing gas entry pressure, and increased permeability once gas became mobile. Therefore, in kaolinite, shear is not an effective self-sealing mechanism for gas flow.

All observations reported are from a pure, saturated, and kaolinite fault gouge. Further investigation is needed in order to confirm gas transport properties in fractures of representative rocks from different disposal concepts.

Acknowledgments

The study was undertaken by staff of the Minerals and Waste Program of the BGS using the experimental facilities of the Transport Properties Research Laboratory (TPRL). Funding for the study was provided by the Nuclear Decommissioning Authority-Radioactive Waste Management Directorate (NDA-RWMD; now the Radioactive Waste Management Limited, RWM), the European Union (FORGE Project; grant agreement 230357) and the British Geological Survey. The authors would like to thank the skilled staff of the Research and Development Workshops at the BGS, in particular Humphrey Wallis, for their design and construction of the experimental apparatus. The authors would also like to thank the reviewers for their helpful comments. This paper is published with the permission of the Director, British Geological Survey (NERC). The data for this paper are available from BGS.

References

Barton, C. A., M. D. Zoback, and D. Moos (1995), Fluid flow along potentially active faults in crystalline rock, *Geology*, *23*(8), 683–686.

Berge, P. A., S. C. Blair, and H. F. Wang (1999), Thermomechanical effects on permeability for a 3-D model of YM rock, in *Proceedings of the 37th U. S. Rock Mechanics Symposium*, edited by B. Amadei et al., pp. 729–734, A. A. Balkema, Rotterdam, Netherlands.

Bossart, P., P. M. Meier, A. Moeri, T. Trick, and J.-C. Mayor (2002), Geological and hydraulic characterisation of the excavation disturbed zone in the Opalinus Clay of the Mont Terri Rock Laboratory, *Eng. Geol.*, *66*(1–2), 19–38.

Crawford, B. R., D. R. Faulkner, and E. H. Rutter (2008), Strength, porosity, and permeability development during hydrostatic and shear loading of synthetic quartz-clay fault gouge, *J. Geophys. Res.*, *113*, B03207, doi:10.1029/2006JB004634.

Cuss, R. J., A. Milodowski, and J. F. Harrington (2011), Fracture transmissivity as a function of normal and shear stress: First results in Opalinus clay, *Phys. Chem. Earth*, *36*, 1960–1971.

Cuss, R. J., S. Sathar, and J. F. Harrington (2012), Fracture transmissivity test in Opalinus Clay, *British Geological Survey Commissioned Report CR/12/132*, 63 pp.

Cuss, R. J., S. Sathar, and J. F. Harrington (2013), Validation of critical stress theory applied to repository concepts, *British Geological Survey Commissioned Report CR/13/001*, 105 pp.

Evans, K. F. (2005), Permeability creation and damage due to massive fluid injections into granite at 3.5 km at Soultz: 2. Critical stress and fracture strength, *J. Geophys. Res.*, *110*, B04204, doi:10.1029/2004JB003169.

Ferrill, D. A., J. Winterle, G. Wittmeyer, D. Sims, S. Colton, A. Armstrong, and A. P. Morris (1999), Stressed rock strains groundwater at Yucca Mountain, Nevada, *GSA Today*, *9*, 1–8.

Finkbeiner, T., C. A. Barton, and M. D. Zoback (1997), Relationships among in-situ stress, fractures and faults, and fluid flow: Monterey, formation, Santa Maria Basin, California, *AAPG Bull.*, *81*, 1975–1999.

Heffer, K., and J. Lean (1993), Earth stress orientation—A control on, and guide to, flooding directionality in a majority of reservoirs, in *Reservoir Characterization III*, pp. 799–822, PennWell Books, Tulsa, Okla.

Horseman, S. T., J. F. Harrington, and P. Sellin (1999), Gas migration in clay barriers, *Eng. Geol.*, *54*, 139–149.

Ito, T., and M. D. Zoback (2000), Fracture permeability and in situ stress to 7 km depth in the KTB scientific drillhole, *Geophys. Res. Lett.*, *27*, 1045–1048, doi:10.1029/1999GL011068.

Laubach, S. E., J. E. Olson, and J. F. W. Gale (2004), Are open fractures necessarily aligned with maximum horizontal stress?, *Earth Planet. Sci. Lett.*, *222*(1), 191–195.

Matilla, J., and E. Tammisto (2012), Stress-controlled fluid flow in fractures at the site of a potential nuclear waste repository, Finland, *Geology*, *40*(4), 299–302.

Ortiz, L., G. Volckaert, P. De Canniére, M. Put, M. A. Sen, S. T. Horseman, J. F. Harrington, M. Impey, and S. Einchcomb (1997), MEGAS: Modelling and experiments on gas migration in repository host rocks, *Final Rep.-Phase 2, EUR 17453 EN*, 155 pp., European Commission, Nuclear Science and Technology, Brussels.

Rogers, S. F. (2003), Critical stress-related permeability in fractured rocks, in *Fracture and In-Situ Stress Characterisation of Hydrocarbon Reservoirs*, edited by M. Ameen, *Geol. Soc. London Spec. Publ.*, *209*, 7–16.

Rogers, S. F., and C. J. Evans (2002), Stress-dependent flow in fractured Rocks at Sellafield, United Kingdom, in *Geological Applications of Well Logs*, edited by M. Lovell and N. Parkinson, *AAPG Methods in Exploration*, *13*, 241–250.

Rutqvist, J., and O. Stephansson (2003), The role of hydromechanical coupling in fractured rock engineering, *Hydrogeol. J.*, *11*, 7–40.

Rutqvist, J., L. Börgesson, M. Chijimatsu, J. Hernelind, L. Jing, A. Kobayashi, and S. Nguyen (2009), Modeling of damage, permeability changes and pressure responses during excavation of the TSX tunnel in granitic rock at URL, Canada, *Environ. Geol.*, *57*(6), 1263–1274.

Sathar, S., H. J. Reeves, R. J. Cuss, and H. J. Harrington (2012), Critical stress theory applied to repository concepts; the importance of stress tensor and stress history in fracture flow, *Mineral. Mag.*, *76*(8), 3165–3177.

Talbot, C. J., and M. Sirat (2001), Stress control of hydraulic conductivity in fracture-saturated Swedish bedrock, *Eng. Geol.*, *61*, 145–153.

Wikramaratna, R. S., M. Goodfield, W. R. Rodwell, P. J. Nash, and P. J. Agg (1993), A preliminary assessment of gas migration from the copper/steel canister, *SKB Tech. Rep. TR93-31*.

Wiseall, A. C., R. J. Cuss, J. F. Harrington, and C. C. Graham (2014), The visualization of flow-paths in experimental studies of clay rich rocks, Geodisposal 2014, 24th – 26th June, 2014, Manchester, U. K.